Polar amplification in idealized climates: the role of ice, moisture, and seasons

Nicole Feldl[1], **Timothy M. Merlis**[2]

[1]Department of Earth and Planetary Sciences, University of California, Santa Cruz, CA, USA
[2]Department of Atmospheric and Oceanic Sciences, McGill University, Montreal, QC, Canada

Key Points:

- Ice thermodynamics promotes a realistic seasonality of polar warming that is greatest in winter.
- Moist energy transport and the ice-albedo feedback make comparable and nearly additive contributions to polar-amplified warming.
- The seasonal cycle of insolation has no impact on annual-mean polar amplification with a simple ice-albedo feedback.

Corresponding author: Nicole Feldl, nfeldl@ucsc.edu

Abstract

The drivers of polar amplification are investigated by isolating the role of sea-ice processes, moist energy transport, and the seasonal cycle of insolation in two models, an energy balance model and an idealized general circulation model. Compared to a simple ice-albedo feedback (temperature-dependent surface albedo), the addition of thermodynamic-ice processes and the seasonal cycle of insolation profoundly affects seasonal polar warming. Climatologically limited-extent ice in the warm season permits only small increases in absorbed solar radiation, producing weak warming, while thick, cold ice in the cold season enables a large radiatively forced response. Despite this enhanced winter warming, the annual-mean polar amplification is modestly reduced by thermodynamic-ice processes. When latent heat transport is disabled, polar amplification is further reduced by a factor of 1.8 across the range of ice representations, suggestive of a nearly additive warming by ice and moist-transport processes.

Plain Language Summary

Since the 1970s, simulations of climate change have predicted warming that is greatest in polar regions. This polar-amplified warming is ubiquitous, though uncertain in magnitude, in climate models subjected to increases in greenhouse gases and has been variously attributed to the ice-albedo feedback, associated with the retreat of reflective sea ice; the lapse rate feedback, associated with the uneven warming of the Arctic atmosphere; and changes in heat transport by atmospheric circulations. In this study, we turn to highly simplified climate models to isolate the role of sea ice and moisture transport on polar amplification and to explore their interactions. We find that, in order to reproduce the seasonality of polar warming in a manner consistent with both observations and state-of-the-art climate models, it is necessary to model the changing thickness of sea ice and not just its retreat. This effect works in concert with moisture transport by the atmosphere to further enhance polar amplification. Together, the findings imply that sea-ice loss leads to winter warming that would promote a positive lapse rate feedback and that the increase in moist energy transport would also lead, in more complex models, to additional warming by increasing the water-vapor greenhouse effect.

1 Introduction

Polar amplification has been a robust projection since the earliest climate simulations; nevertheless, the magnitude and timing of the surface warming at high latitudes remains poorly constrained. The phenomenon has been variously attributed to the ice-albedo feedback (e.g., Manabe & Wetherald, 1975), to an increase in poleward atmosphere-ocean energy transport (e.g., Holland & Bitz, 2003; Hwang et al., 2011), and to temperature feedbacks (e.g., Winton, 2006; Pithan & Mauritsen, 2014). Recent work has highlighted the interconnected nature of positive albedo and lapse rate feedbacks over sea-ice regions: summer sea-ice loss increases absorbed solar radiation, and the seasonal transfer of energy by ocean heat storage drives, in the presence of stable atmospheric stratification, surface-enhanced winter warming (Laîné et al., 2016; Boeke & Taylor, 2018; Dai et al., 2019; Feldl et al., 2020). Hence the uncertainty in projections of climate change, commonly expressed as intermodel spread, arises in part from incomplete understanding of the interaction among these processes. While simple models tend to emphasize that poleward energy transport *can* produce polar-amplified warming purely through moist atmospheric processes (e.g., Roe et al., 2015; Merlis & Henry, 2018), they often neglect critical real-world physics such as ice thermodynamics and seasonal variations in insolation. Investigation of a current gap in the modeling hierarchy—that of the idealized moist, icy, and seasonal climate model—reveals how energy transport and sea-ice processes work in concert to produce latitudinally and seasonally varying warming.

For our idealized climate models, we consider both energy balance models (EBMs) and general circulation models (GCMs). Traditional EBMs represent atmospheric energy transport as a diffusive process proportional to the meridional gradient of temperature and include the ice-albedo feedback via a temperature-dependent surface albedo (Budyko, 1969; Sellers, 1969; North, 1975; North et al., 1981). As a consequence of these parametrizations, when subject to a uniform radiative forcing, the simulated warming is greatest at polar latitudes. When the ice albedo is locked (Merlis, 2014) or the ice-albedo feedback disabled (Armour et al., 2019), warming is uniform, and every latitude warms by the reference climate sensitivity. Thus polar amplification in the dry EBM requires spatial heterogeneity in radiative feedbacks or radiative forcing in order to drive changes in atmospheric energy transport. The results of the early modeling studies in particular have contributed to the prevailing view that polar amplification requires the presence of sea-ice processes.

The rise of the moist EBM in recent years has challenged the necessity of polar feedbacks in producing polar-amplified warming. In the moist EBM, moist static energy replaces temperature in the calculation of diffusive energy transport, which allows for an increase in the latent component of energy transport with warming (Flannery, 1984). Accounting for the effects of latent heat on energy transport improves the ability of EBMs to mimic the zonal-mean behavior of GCMs. Further, in contrast to their dry counterparts, moist EBMs produce polar amplification even in the absence of spatially varying radiative forcing or feedbacks (Roe et al., 2015). This behavior can be understood as a result of the preferential increase in tropical water vapor with warming that, combined with down-gradient moist static energy diffusion, produces an increase in atmospheric energy transport. Moist EBMs can be coupled to a sea-ice parametrization (e.g., Lutsko et al., 2020), prescribed with surface albedo changes (e.g., Hwang & Frierson, 2010), or neither (e.g., Merlis & Henry, 2018). Not surprisingly, when the ice-albedo feedback is enabled in one form or another, polar amplification is enhanced. We also note that two varieties of the moist EBM implementation are in common usage: a climatological version that integrates the governing equation numerically and does not prescribe patterns of feedbacks (Frierson et al., 2007; Merlis & Henry, 2018) and a perturbation version cast in terms of meridional patterns of radiative forcing, radiative feedbacks, ocean heat uptake, and anomalous moist static energy (Rose et al., 2014; Roe et al., 2015; Bonan et al., 2018; Armour et al., 2019). In this study we build upon the former so that sea ice is an interactive component of the climate system, allowing it to shape the control climate and the response to warming.

Like moist EBMs, idealized GCMs tend to produce polar amplification in the absence of sea-ice processes (Alexeev et al., 2005; Langen et al., 2012; Russotto & Biasutti, 2020), though the result is not ubiquitous and is likely model dependent (Feldl et al., 2017). For instance, Kim et al. (2018) showed, in an aquaplanet simulation with no ice-albedo feedback, that climate feedbacks depend on insolation conditions, with a positive polar lapse rate feedback contributing to a strongly polar-amplified response in perpetual equinox and a negative polar cloud feedback cancelling polar warming given seasonally varying insolation. A number of questions arise regarding the fundamental role of seasonality in polar amplification that, given the disparity of previous results, warrant systematic investigation: Does the seasonal cycle of insolation affect annual-mean polar amplification in highly idealized models? What processes drive the seasonal manifestation of polar amplification? Further, given the well-known stabilizing effect of sea-ice thermodynamic processes (i.e., a growth-rate dependence on ice thickness that promotes rapid recovery of thin ice to perturbations; Bitz & Roe, 2004; Eisenman & Wettlaufer, 2009), how does seasonally varying sea-ice thickness influence polar amplification?

Evidence from models of various complexities suggest that local climate feedbacks work in concert with moist atmospheric processes to consistently produce polar-amplified warming. In what follows, we systematically isolate the role of sea-ice processes, moist

energy transport, and the seasonal cycle of insolation on polar amplification. We advance prior studies by incorporating the seasonal dynamics of sea ice in a moist EBM and idealized GCM, and we investigate how the annual and seasonal polar response differs in the presence of thermodynamic ice versus a simple ice-albedo feedback enabled by a temperature-dependent surface albedo. Of particular interest is the potential for additive or offsetting behavior of the different mechanisms contributing to polar amplification. In other words, we seek to determine how the magnitude of polar amplification is controlled by ice and moist-transport processes both combined and in isolation.

2 Methods

2.1 Moist EBM

The EBM used in this study, at its most comprehensive level, includes seasonal variations in climate, an idealized representation of sea-ice thickness and albedo, and an idealized representation of atmospheric energy transport as a moist diffusive process. The model evolves surface enthalpy, $E(x,t)$ where x is sine of latitude, which represents the energy stored in the ocean mixed layer as sensible heat when the ocean is ice free or in sea ice as latent heat when the ocean is ice covered:

$$\frac{\partial E}{\partial t} = aS - (A + BT) - \nabla \cdot F_a + \mathcal{F}, \tag{1}$$

with surface temperature T, net solar radiation aS, outgoing longwave radiation (OLR) $A+BT$, divergence of atmospheric energy transport $\nabla \cdot F_a$, and uniform radiative forcing $\mathcal{F}$. Net solar radiation follows Wagner and Eisenman (2015), where insolation $S(x,t) = S_0 - S_1 x \cos \omega t - S_2 x^2$. The fraction of insolation that is absorbed, a, which depends on solar zenith angle, cloudiness, and surface albedo, is approximated as $a_0 - a_2 x^2$ where $E \geq 0$ (open-water conditions) and a_i where $E < 0$ (ice). We use the following parameter values: $c_w = 7.8$ W yr m^{-2} K^{-1} (i.e., equivalent to a mixed-layer depth of 60 m), $A = 196$ W m^{-2}, $B = 1.8$ W m^{-2}, $S_0 = 420$ W m^{-2}, $S_1 = 338$ W m^{-2}, and $S_2 = 240$ W m^{-2}, $a_0 = 0.7$, $a_2 = 0.1$, and $a_i = 0.4$. In the control simulation, $\mathcal{F} = 0$ W m^{-2}, and it is increased to $\mathcal{F} = 8$ W m^{-2} in the perturbation simulation. The magnitude of the forcing, roughly comparable to a $4\times CO_2$ scenario, is sufficient to for the climate to become ice-free, though the results are qualitatively similar for a smaller amplitude forcing that retains winter ice.

Divergence of atmospheric energy transport is assumed to be proportional to the meridional gradient of near-surface moist static energy (MSE) h:

$$\nabla \cdot F_a(x) = -\frac{\partial}{\partial x} D(1-x^2) \frac{\partial h}{\partial x}, \tag{2}$$

with constant diffusivity $D = 0.3$ W m^{-2} K^{-1}. Building on the work of Wagner and Eisenman (2015), diffusion occurs in a ghost layer with heat capacity $c_g = 0.098$ W yr m^{-2} K^{-1}. In our model, the ghost-layer temperature T_g is relaxed to the surface temperature with time scale $\tau_g = 1 \times 10^{-5}$ yr and evolves according to

$$c_g \frac{\partial T_g}{\partial t} = \frac{c_g}{\tau_g}(T - T_g) + D\nabla^2 T_g + D\nabla^2 c_p^{-1} L_v \mathcal{H} q_s(T_g). \tag{3}$$

MSE is defined in units of temperature as $h = T_g + c_p^{-1} L_v \mathcal{H} q_s(T_g)$ for latent heat of vaporization $L_v = 2.5 \times 10^6$ J kg^{-1}, relative humidity $\mathcal{H} = 0.8$, specific heat of air at constant pressure $c_p = 1004.6$ J kg^{-1} K^{-1}, and saturation vapor pressure q_s. Numerically, this approach enables us to perform an implicit time-stepping method on the diffusion of sensible heat (second term on the right-hand side of (3)) and a forward Euler method on the diffusion of latent heat (third term on the right-hand side of (3)).

Temperature at the top surface of ice, T_0 is determined by the balance between the conductive heat flux upward through the ice and the energy flux

$$\frac{k(T_m - T_0)}{h_i} = -aS + A + B(T_0 - T_m) + \nabla \cdot F_a - \mathcal{F}, \tag{4}$$

with ice thermal conductivity $k = 2$ W m^{-1} K^{-1} and melting point $T_m = 0$°C (Wagner & Eisenman, 2015). From T_0 we determine the ice regime. In the freezing regime, $T_0 < T_m$ and $E < 0$; the energy flux is balanced by subfreezing surface temperature, and $T = T_0$. In the melting regime, $T_0 \geq T_m$ and $E < 0$, and surface temperature remains at the melting point, $T = T_m$. Open-water conditions are included by adding a third surface regime: if $E \geq 0$, $T = E/c_w$ where c_w is the mixed-layer heat capacity. Equation (1) governs both ice-free surface temperature and ice thickness ($h = -E/L_f$).

The EBM simulations use the domain $-1 < x < 1$ with 120 grid points spaced uniformly in x. They are integrated for 100 years with 1000 time steps per year, and we present averages over the last year.

2.2 GCM

The idealized moist GCM builds on the work of Frierson et al. (2006) and includes a gray-radiation atmosphere and an idealized hydrological cycle. Water vapor is advected by the resolved-scale flow, undergoing condensation when supersaturated, and is subject to a simple moist convection parameterization for unresolved convection (Frierson et al., 2007). Insolation varies seasonally according to a circular orbit with Earth's obliquity (23.45°) and a 360-day year. A top-of-atmosphere coalbedo that is a time-independent function of latitude ϕ is given by $a^{TOA} = a_0^{TOA} + \Delta a^{TOA}(3\sin^2\phi - 1)/2$, which represents the atmosphere's contribution, primarily clouds, to the planetary albedo. We use $a_0^{TOA} = 0.68$ and $\Delta a^{TOA} = -0.2$, following North et al. (1981). The step-change in albedo at the ice edge is represented by a temperature-dependent surface albedo (0.4 for subfreezing temperatures and 0.1 elsewhere). The surface boundary condition follows the formulation described above for the EBM, as implemented by Zhang et al. (submitted). Climate changes are forced by varying the longwave optical depth in the gray radiation scheme (O'Gorman & Schneider, 2008). The control simulation optical depth at the surface is a time-independent function of latitude, $\tau_e + (\tau_p - \tau_e)\sin^2\phi$, with $\tau_e = 7.2$ and $\tau_p = 3.6$. The vertical structure of the optical depth is the same as in O'Gorman and Schneider (2008), and the perturbation simulations have a 50% larger optical depth. As in the perturbed EBM climates, this is a sufficient amplitude forcing for the GCM climate to enter a perennial ice-free state.

The GCM simulations use T42 spectral resolution ($\approx 2.8°$ horizontal resolution) with 30 vertical levels. They are integrated for 30 years with a 600 s timestep, and we present averages over the last 20 years.

The GCM closely follows the EBM formulation with the following differences. The insolation and prescribed planetary albedo differ somewhat, though control values of absorbed solar radiation at the top-of-atmosphere are in good agreement (Fig. S1). The GCM atmosphere explicitly simulates atmosphere's large-scale turbulence, in ways that potentially depart from the constant diffusivity formulation of the EBM. The GCM atmosphere additionally has full vertical structure, characterized by near radiative-convective and radiative-advective equilibrium in the tropics and polar regions, respectively. This allows for a lapse rate feedback that varies in sign (Payne et al., 2015). In addition to the lapse rate feedback, the GCM represents a Planck feedback and albedo feedback but no water vapor or cloud feedbacks. Longwave feedbacks in the EBM are encapsulated in the globally uniform B parameter. As a result of these differences, the GCM has a more stabilizing global-mean longwave feedback (-3.7 W m^{-2} K^{-1}) and a weaker destabilizing ice albedo feedback than the corresponding EBM, and hence the magnitude of

the global-mean radiative forcing is roughly three times that of the EBM to produce a comparable climate response.

2.3 Experiment Hierarchy

The models described above are the most comprehensive versions of the "Moist EBM" and GCM presented in this study. Further, we incrementally disable ice thermodynamics, the seasonal cycle of insolation, ice albedo, and the effect of latent energy on the EBM's diffusive representation of atmospheric energy transport in order to assess their relative contributions to polar amplification in our idealized framework:

- *Ice thermodynamics* - Our most comprehensive simulations. In addition to an ice-thickness-dependent surface temperature, they also include a temperature-dependent albedo and hence an ice-albedo feedback.
- *Simple ice-albedo feedback* - Sea-ice thermodynamics are eliminated while retaining the surface-albedo temperature dependence $\alpha(T)$ by evolving the surface enthalpy assuming a surface of 60 m of water and permitting sub-freezing temperatures. Hence, surface temperature is given everywhere by the open-water condition (E/c_w).
- The seasonal cycle is eliminated from the EBM by setting $S_1 = 0$ W m^{-2} and by using the annual-mean of the seasonal insolation for all times in the GCM.
- *Ice-free* - Ice albedo and ice thermodynamics are both eliminated by setting the albedo equal to its spatially varying open-water value and evolving the surface enthalpy for a 60-m mixed-layer ocean that permits sub-freezing temperatures.
- *"Dry EBM"* - In the EBM, the effect of latent energy is eliminated by setting $\mathcal{H} = 0$. The diffusivity D is doubled to 0.6 W m^{-2} K^{-1} to maintain an Earth-like atmospheric energy transport (Flannery, 1984), and OLR parameter A is decreased by 3 W m^{-2}. The Dry EBM is identical to that of Wagner and Eisenman (2015), aside from certain parameter values and a global, rather than single-hemisphere, domain. Ice thermodynamics, the seasonal cycle of insolation, and ice albedo can be additionally eliminated from the Dry EBM.

3 Results

The climate response to a radiative forcing in the Moist EBM and GCM organize into three groupings (Figure 1a,b). Climate change with a simple ice-albedo feedback, either with or without seasons, exhibits the greatest polar amplification. The addition of ice thermodynamics with seasons reduces warming at all latitudes and reduces polar amplification, particularly in the EBM. When ice thermodynamics without seasons is included, on the other hand, the response is identical (GCM) and nearly identical (EBM) to the climate response with a simple ice-albedo feedback (not shown), and in what follows we limit the thermodynamic-ice simulations to the seasonal case only. The amount of polar amplification for these icy regimes is comparable between the EBM and GCM, with a polar amplification factor of 3-4.

Climate change in the absence of ice, either with or without seasons, is characterized by less polar amplification than in the presence of ice feedbacks (orange lines in Fig. 1a,b). The result that polar amplification is merely reduced rather than eliminated is consistent with prior studies with moist EBMs (Roe et al., 2015; Merlis & Henry, 2018; Armour et al., 2019). However, that reduction is substantially less in the GCM, which overall exhibits less range in climate responses. Because the change in net solar radiation is zero in the ice-free EBM and GCM, the different responses must ultimately derive from differences in the model representations of atmospheric energy transport (i.e., diffusive in the EBM versus macroturbulent in the GCM) or the presence of spatially varying temperature feedbacks in the GCM, particularly the lapse rate feedback (Fig.

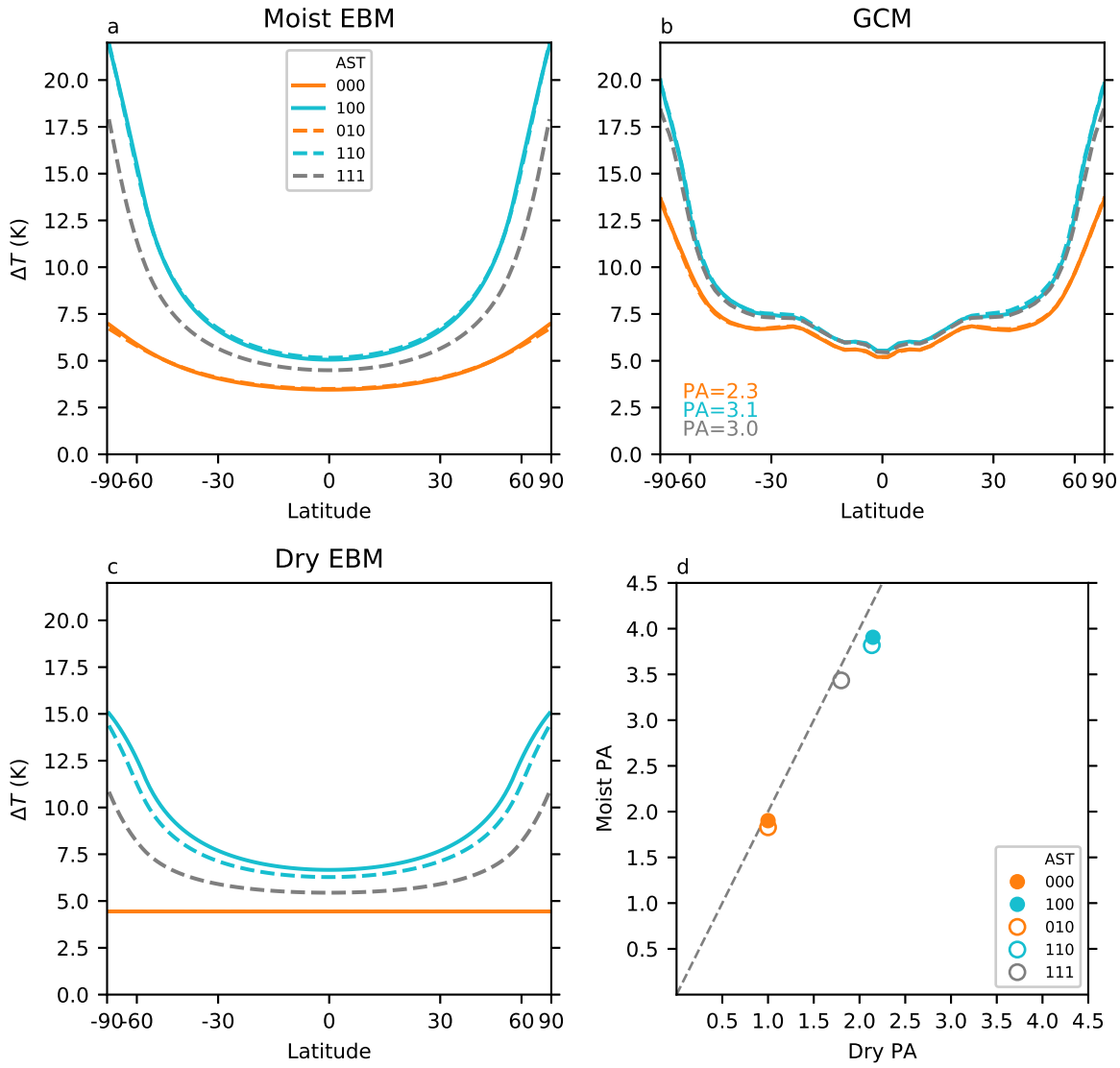

Figure 1. Polar amplification in the Moist EBM, GCM, and Dry EBM. (a) Annual-mean temperature response to an 8 W m^{-2} radiative forcing in the Moist EBM. (b) Annual-mean zonal-mean surface air temperature response to a 50% increase in longwave optical thickness in the GCM. (c) Annual-mean temperature response to an 8 W m^{-2} radiative forcing in the Dry EBM. (d) Polar amplification in the Moist EBM compared to the Dry EBM, where the grey dashed reference line has a slope of 2. The polar amplification factor (PA) is calculated as the ratio of polar (65-90N) to tropical (0-6N) warming. Simulation codes in the legend indicate whether ice albedo (A), seasonal cycle of insolation (S), or ice thermodynamics (T) are active: 000 (ice free), 010 (ice free with seasons), 100 (simple ice-albedo feedback), 110 (simple ice-albedo feedback with seasons), 111 (ice thermodynamics with seasons).

S2). Notably, the inclusion of seasons in these idealized simulations has no effect on the magnitude and structure of annual-mean warming.

To understand why polar amplification is reduced by thermodynamic-ice processes, we compare the seasonal cycle of temperature change across the sub-hierarchy of icy simulations (Fig. 2). We begin with the Moist EBM response and below highlight the broad similarities to the GCM response. The reduced amplification is clearly revealed to be a warm-season phenomenon (Fig. 2b,c). Examination of the climatological position of the ice line (black line in Fig. 2) shows that thermodynamic ice has greater seasonal variability: the seasonal sea-ice maximum extends to the same latitude as for a simple ice-albedo feedback, however, the seasonal sea-ice minimum exhibits climatologically less ice. Hence, when subjected to a radiative forcing, there is less ice retreat, a smaller increase in net solar radiation (Fig. 3a,b), and less polar warming broadly across the warm season. We note this weak warming arises from a different source than the late spring/early summer absolute minimum near the pole, which is more limited in extent and occurs where seasonal climatological temperatures are at their maximum and radiatively forced warming at its minimum.

In contrast, during the cold season, polar amplification is enhanced by thermodynamic-ice processes. This disparate response is due not to a greater increase in net solar radiation (they are the same; Fig. 3a,b), nor to a weaker decrease in polar MSE flux convergence (it is stronger; Fig. 3e,f). Rather, the presence of ice thermodynamics results in a much colder base climate state, necessitating a larger temperature change when that ice melts (Fig. 3i). When the ice loss is prescribed as a forcing (Fig. 2d), the response explains essentially all of the warm-season polar warming and in the cold season is approximately 4 K less than the total response to a radiative forcing (cf. Fig. 2c). The difference between Figure 2c and 2d is the warming that occurs when ice is locked to its climatological location and thickness (Fig. S3). While climatological differences in surface heat capacity between seasonally ice-free and ice-covered regions will promote winter-enhanced warming in the absence of ice loss, the seasonal range of polar warming in the locked-ice experiment is only 4 K, compared to 28 K for the total response, indicating the predominant role of ice-thickness changes.

The two key characteristics of thermodynamic ice—small ice extent during the warm season and thick, cold ice during the cold season—are both a consequence of the nonlinear growth rate of ice (4). Thin ice grows *and* melts faster than thick ice. However, the melt case is limited because once T_0 warms to the melting point, $T = T_m$. Freezing ice has no such temperature constraint, and surface temperature monotonically decreases with ice thickness. Hence, the effect of ice thermodynamics is to permit large seasonal excursions in ice extent characterized by summer temperatures near the melting point and by thick cold-season ice with surface temperatures substantially below the freezing point. The latent heating of seasonally melting ice modulates the timing and magnitude of the forced response but does not fundamentally determine it; simulations in which the melting regime (cyan line, Fig. 2c) is limited by varying the S_1 parameter still exhibit a summertime polar warming minimum. As noted by Eisenman and Wettlaufer (2009), the growth-rate nonlinearity also supports stable seasonally ice-free climate states. Indeed, in simulations with more modest climate changes where ice persists in the cold season (not shown), the same mechanism determining the seasonal cycle of temperature change applies. The small-forcing warming pattern is thus also characterized by weak warm-season warming and, when cold-season ice thins and partially retreats, enhanced warming.

The seasonal cycle of polar amplification manifests differently with a simple ice-albedo feedback. The seasonal amplitude of polar warming is small and reaches its maximum in the warm season and its minimum in the cold season (Fig. 2b). A warm-season polar warming maximum can be explained by substantial ice retreat and, as a consequence, a large increase in net solar radiation (Fig. 3a). Additionally, the increase in absorbed

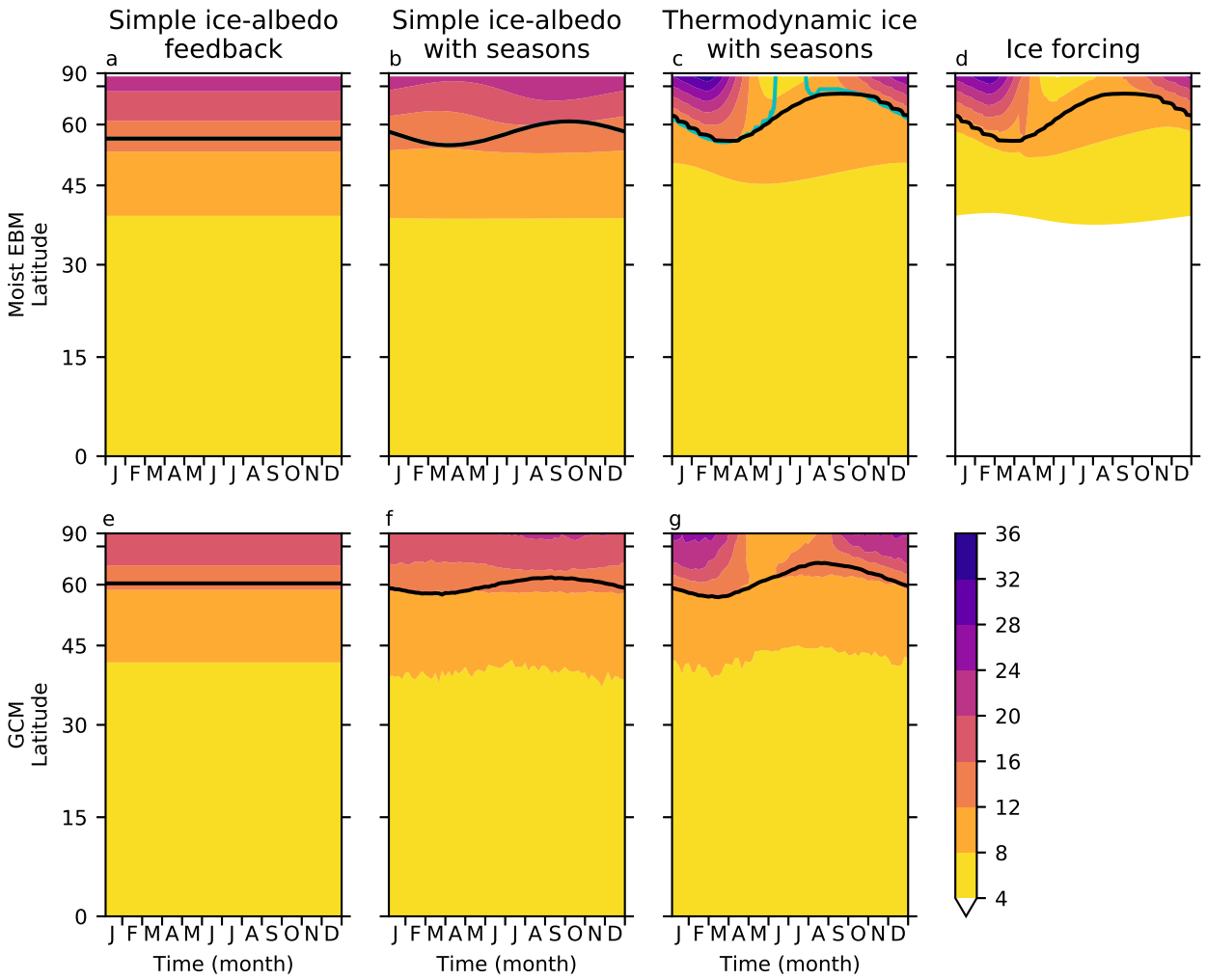

Figure 2. Seasonal cycle of temperature change in the Moist EBM and GCM in the presence of (a,e) a simple ice-albedo feedback (annual-mean insolation), (b,f) a simple ice-albedo feedback, and (c,g) ice thermodynamics. The black contour is the position of the climatological ice line ($h_i = 0$ m or $T = 0^\circ$C contour). The cyan contour defines the climatological melting regime ($T_0 = 0^\circ$C). As in Fig. 1, the GCM's surface air temperature is shown. (d) Seasonal cycle of temperature change for prescribed ice loss and constant radiative forcing ($\mathcal{F} = 8$ W m^{-2}). The temperature response to ice forcing is calculated as the difference between a Moist EBM simulation with freely evolving thermodynamic ice and a simulation with ice locked to its mean-state location and thickness.

solar radiation goes directly to raising temperatures rather than to melting ice. In neglecting the thermodynamic-ice processes described above, the seasonality of warming becomes inconsistent with comprehensive simulations and observations of polar warming. Hence, caution should be exercised when applying the moist, seasonal EBM with a simple ice-albedo feedback beyond the annual-mean climate response.

The seasonal cycle of temperature change in the GCM sub-hierarchy (Fig. 2, bottom) is broadly consistent with the Moist EBM. For a simple ice-albedo feedback, the seasonal cycle of ice extent is muted (black line, Fig. 2f), and extensive ice retreat occurs in all seasons. Polar warming is greatest in the warm season, attendant with a relatively large increase in TOA net SW radiation (Fig. 3c). The change in net solar radiation is smaller in the GCM than the EBM due to differences in the implementation of insolation and planetary albedo discussed in Section 2. Including thermodynamic-ice processes makes conditions less favorable for the maintenance of warm-season ice in the mean state (black line, Fig. 2g). Hence, the increases in TOA net SW radiation (Fig. 3d) and temperature (Fig. 2g) are relatively weak in the warm season, and it is the loss of thick cold-season ice (Fig. 3j) that produces substantial polar warming. In contrast to the Moist EBM, the summer polar warming in the GCM is not as strongly reduced by the presence of ice thermodynamics, and, accordingly, the annual-mean temperature changes are less sensitive to different representations of ice processes (Fig. 1). Additionally, summer exhibits a substantial increase in convergence of MSE flux into polar regions that is absent for a simple ice-albedo feedback (Fig. 3g,h). The seasonal transition from enhanced to reduced convergence is consistent with the much greater weakening of MSE gradients under strong cold-season polar amplification.

We disable latent heat transport to elucidate the extent to which moist atmospheric processes and sea-ice processes interact to determine annual-mean polar amplification. In the Dry EBM, polar amplification is reduced across the hierarchy (Fig. 1c). The poles systematically warm less, and the tropics warm more. The previously identified groupings remain: climate change with a simple ice-albedo feedback exhibits greatest polar amplification, climate change with ice thermodynamics exhibits moderate polar amplification, and climate change in the absence of ice produces no polar amplification. As before, the presence of seasons has no effect on the structure of warming. Notably, polar amplification in the Dry EBM is approximately half that of the Moist EBM. If the ice-albedo feedback and latent heat transport were perfectly additive in their contributions to polar amplification, then we would expect each to produce, for instance, a doubling and their combined contribution to produce a quadrupling; in other words, we would expect the amplification factors in Figure 1d to fall along the 2:1 line. Starting from the ice-free Dry EBM with seasons (PA $= 1$), adding latent heat transport and adding a simple ice-albedo feedback both nearly double polar amplification (PA $= 1.8$ and PA $=$ 2.2, respectively), and their combined influence (PA $= 3.8$) is slightly less than their sum. A linear least-squares regression yields a slope of 1.8 across the entire range of simulations (not shown).

4 Conclusions

In this study, we have exploited a gap in climate model simulations to elucidate the role of, and interactions between, ice processes, the seasonal cycle, and moist processes in determining the polar-amplified pattern of warming. Further, we systematically compare the representation of the atmospheric flow: an idealized global circulation model resolves the atmospheric macroturbulence, while a diffusive energy balance model represents the net effect of this large-scale turbulence as a down-gradient, diffusive process. These simulations reveal that the inclusion of an ice-albedo feedback via a simple temperature-dependent surface albedo promotes polar amplification in the annual mean, as expected, however, the seasonal cycle of the temperature response exhibits a warm-season maximum that is inconsistent with comprehensive climate model projections. Adding com-

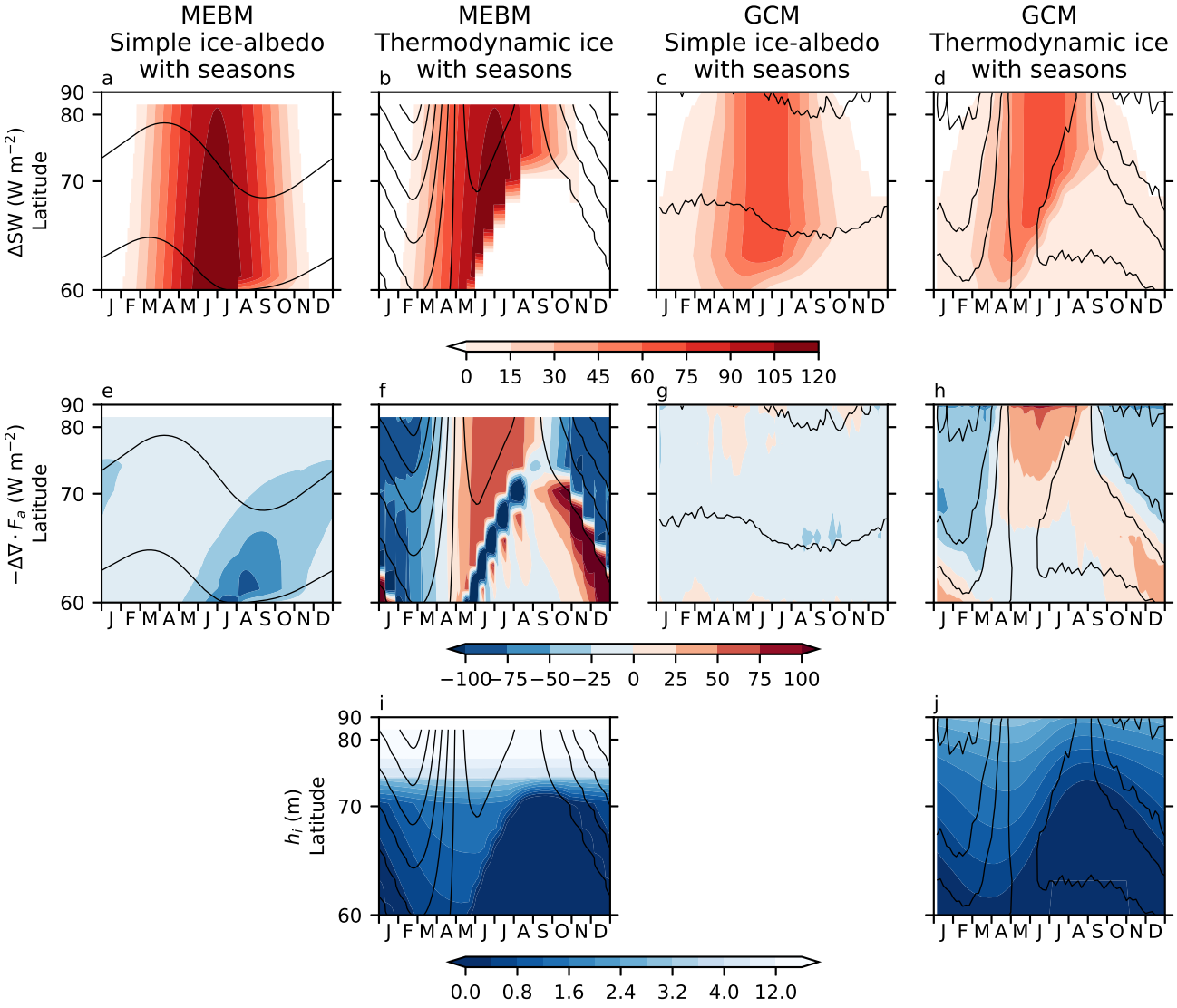

Figure 3. Change in polar energy flux diagnostics and climatological ice thickness for the Moist EBM and GCM. (a-d) Change in TOA net shortwave radiation in the presence of a simple ice-albedo feedback and ice thermodynamics. (e-h) Change in convergence of MSE flux for the same simulations as in (a-d), with a one-month running mean applied to the GCM polar-average change in MSE flux convergence. (i,j) Climatological ice thickness in simulations with ice thermodynamics. Black lines in all panels reproduce the temperature change contours shown in Fig. 2.

plexity to the sea-ice processes in the form of a conductive heat flux upward through the ice modestly offsets the annual-mean polar-amplified warming and profoundly affects the seasonal cycle of polar-amplified warming. In these thermodynamic-ice simulations, enhanced winter warming occurs in both the EBM and GCM, a finding previously identified by Held (1982).

The seasonal cycle of insolation has essentially no effect on annual-mean polar amplification (in contrast to comprehensive models that include cloud radiative feedbacks, e.g., Kim et al., 2018) and little effect on the seasonality of polar-amplified warming—until sea-ice thermodynamic processes are included. Here, the seasonal polar warming arises as a consequence of the climatological ice state, which is characterized by large seasonal excursions in ice extent and thickness. Hence, under radiatively forced warming, the melting of thick ice produces a large winter temperature response (referred to, by Manabe and Stouffer (1980), as a reduction in the thermal insulation effect of sea ice), and in the climatologically ice-free region there can be no change in net solar radiation, limiting warming in the warm season. The stronger seasonality of polar-amplified warming in the EBM is consistent with the greater amount of ice thinning. Thick sea ice has a small effective heat capacity that produces large seasonal variations in temperature. All else being equal, the climate transition from thick ice to water, as illustrated in the EBM, will be characterized by larger reductions in seasonal temperature variations. The weaker seasonal warming variability in the GCM is consistent with a transition from relatively thin ice to water.

The role of moist energy transport is critical in giving rise to polar-amplified warming in the absence of ice feedbacks, consistent with prior studies (Roe et al., 2015; Merlis & Henry, 2018; Armour et al., 2019). Furthermore, the Moist EBM simulations have a factor of 1.8 greater polar amplification across the range of representations of ice processes relative to corresponding Dry EBM simulations. This is suggestive of a superposition: in isolation, ice processes amplify polar warming; in isolation, moist processes amplify polar warming; together, ice and moist processes lead to amplified polar warming that is comparable to the sum of the individual roles. Through our mechanism-denial experiment, we clearly demonstrate the warming effect of latent heat transport, which is often obscured in intermodel analyses where large decrease in dry static energy transport tend to produce an anti-correlation between polar amplification and change in atmospheric energy transport (e.g. Hwang et al., 2011). Additionally, while the more sophisticated treatment of atmospheric dynamics and radiation quantitatively influences the annual-mean polar amplification, qualitative sensitivities to different ice representations are similar in the EBM and GCM. Notably, in these simulations moist transport can directly influence polar warming, however, it cannot influence warming via the water vapor feedback (e.g., Henry et al., 2021) or cloud feedbacks (Yoshimori et al., 2017; Graversen & Langen, 2019).

In summary, our systematic investigations in two idealized models reveal how all three mechanisms, ice processes, moist processes, and the seasonal cycle of insolation, drive the annual-mean and, importantly, seasonal pattern of polar-amplified warming. While the seasonal insolation cycle has no effect on the annual-mean polar amplification with a simple ice-albedo feedback, neglecting it results in a lack of fidelity of the seasonal cycle of warming with respect to projections from comprehensive models. Furthermore, the seasonal solar forcing is fundamental in setting the climatological thermodynamic ice state that preconditions the ice-albedo feedback under more realistic ice representations. That feedback is weaker than that of a simple ice-albedo feedback and would contribute less to polar warming using popular TOA diagnostic frameworks (e.g., Pithan & Mauritsen, 2014). However, the weak surface albedo feedback conceals large seasonal changes in temperature, demonstrating, in the EBM, that stable stratification and a positive lapse rate feedback are not requirements for winter-enhanced warming, because the EBM has neither. If a positive polar lapse rate feedback is present, as in the GCM, then

thermodynamic-ice processes act to enhance it. The important role of the climatological ice extent also suggests a reason for the success of perturbation EBMs, which include it implicitly when prescribing CMIP-derived albedo feedbacks. While questions remain regarding cloud interactions, our findings of comparable and nearly additive contributions of the ice-albedo feedback and moist transport provide a basis for refined assessment of attributions of Arctic amplification.

Acknowledgments

We are grateful to Till Wagner, Ian Eisenman, and Xiyue (Sally) Zhang for providing EBM and GCM codes that enabled this research. We thank Ian Eisenman for helpful discussions about the model numerics and Patrick Taylor for galvanizing the research. Support was provided by National Science Foundation award AGS-1753034 (NF) and a Compute Canada/Canada Foundation for Innovation computing allocation and a Canada Research Chair (TMM). Data and code supporting this research are available at

https://doi.org/10.5281/zenodo.5176662.

References

Alexeev, V. A., Langen, P. L., & Bates, J. R. (2005). Polar amplification of surface warming on an aquaplanet in "ghost forcing" experiments without sea ice feedbacks. *Climate Dynamics*, *24*, 655–666. doi: 10.1007/s00382-005-0018-3

Armour, K. C., Siler, N., Donohoe, A., & Roe, G. H. (2019). Meridional atmospheric heat transport constrained by energetics and mediated by large-scale diffusion. *Journal of Climate*, *32*(12), 3655–3680. doi: 10.1175/JCLI-D-18-0563.1

Bitz, C. M., & Roe, G. H. (2004). A mechanism for the high rate of sea ice thinning in the Arctic Ocean. *Journal of Climate*, *17*(18), 3623–3632. doi: 10.1175/1520-0442(2004)017⟨3623:AMFTHR⟩2.0.CO;2

Boeke, R. C., & Taylor, P. C. (2018). Seasonal energy exchange in sea ice retreat regions contributes to differences in projected Arctic warming. *Nature Communications*, *9*. doi: 10.1038/s41467-018-07061-9

Bonan, D. B., Armour, K. C., Roe, G. H., Siler, N., & Feldl, N. (2018). Sources of uncertainty in the meridional pattern of climate change. *Geophysical Research Letters*, *45*, 9131–9140. doi: 10.1029/2018GL079429

Budyko, M. I. (1969). The effect of solar radiation variations on the climate of the Earth. *Tellus*, *21*, 611–619. doi: 10.3402/tellusa.v21i5.10109

Dai, A., Luo, D., Song, M., & Liu, J. (2019). Arctic amplification is caused by sea-ice loss under increasing CO2. *Nature Communications*, *10*, 121. doi: 10.1038/s41467-018-07954-9

Eisenman, I., & Wettlaufer, J. S. (2009). Nonlinear threshold behavior during the loss of Arctic sea ice. *Proceedings of the National Academy of Sciences of the United States of America*, *106*(1), 28–32. doi: 10.1073/pnas.0806887106

Feldl, N., Bordoni, S., & Merlis, T. M. (2017). Coupled high-latitude climate feedbacks and their impact on atmospheric heat transport. *Journal of Climate*, *30*(1), 189–201. doi: 10.1175/JCLI-D-16-0324.1

Feldl, N., Po-Chedley, S., Singh, H. K., Hay, S., & Kushner, P. J. (2020). Sea ice and atmospheric circulation shape the high-latitude lapse rate feedback. *npj Climate and Atmospheric Science*, *3*. doi: 10.1038/s41612-020-00146-7

Flannery, B. P. (1984). Energy balance models incorporating transport of thermal and latent energy. *Journal of the Atmospheric Sciences*, *41*(3), 414–421. doi: 10.1175/1520-0469(1984)041⟨0414:EBMITO⟩2.0.CO;2

Frierson, D. M. W., Held, I. M., & Zurita-Gotor, P. (2006). A gray-radiation aquaplanet moist GCM. Part I: Static stability and eddy scale. *Journal of the Atmospheric Sciences*, *63*(10), 2548–2566. doi: 10.1175/JAS3753.1

Frierson, D. M. W., Held, I. M., & Zurita-Gotor, P. (2007). A gray-radiation aquaplanet moist GCM. Part II: Energy transports in altered climates. *Journal of the Atmospheric Sciences*, *64*(5), 1680–1693. doi: 10.1175/JAS3913.1

Graversen, R. G., & Langen, P. L. (2019). On the role of the atmospheric energy transport in 2×CO2-induced polar amplification in CESM1. *Journal of Climate*, *32*(13), 3941–3956. doi: 10.1175/JCLI-D-18-0546.1

Held, I. M. (1982). Climate models and the astronomical theory of the ice ages. *Icarus*, *50*(2-3), 449–461. doi: 10.1016/0019-1035(82)90135-X

Henry, M., Merlis, T. M., Lutsko, N. J., & Rose, B. E. (2021). Decomposing the Drivers of Polar Amplification with a Single Column Model. *Journal of Climate*, *34*(6), 2355–2365. doi: 10.1175/jcli-d-20-0178.1

Holland, M. M., & Bitz, C. M. (2003). Polar amplification of climate change in coupled models. *Climate Dynamics*, *21*, 221–232. doi: 10.1007/s00382-003-0332-6

Hwang, Y.-T., & Frierson, D. M. W. (2010). Increasing atmospheric poleward energy transport with global warming. *Geophysical Research Letters*, *37*(24). doi: 10.1029/2010GL045440

Hwang, Y.-T., Frierson, D. M. W., & Kay, J. E. (2011). Coupling between Arctic feedbacks and changes in poleward energy transport. *Geophysical Research Letters*, *38*(17). doi: 10.1029/2011GL048546

Kim, D., Kang, S. M., Shin, Y., & Feldl, N. (2018). Sensitivity of polar amplification to varying insolation conditions. *Journal of Climate*, *31*(12), 4933–4947. doi: 10.1175/JCLI-D-17-0627.1

Laîné, A., Yoshimori, M., & Abe-Ouchi, A. (2016). Surface Arctic Amplification Factors in CMIP5 Models: Land and Oceanic Surfaces and Seasonality. *Journal of Climate*, *29*(9), 3297–3316. doi: 10.1175/JCLI-D-15-0497.1

Langen, P. L., Graversen, R. G., & Mauritsen, T. (2012). Separation of contributions from radiative feedbacks to polar amplification on an aquaplanet. *Journal of Climate*, *25*(8), 3010–3024. doi: 10.1175/JCLI-D-11-00246.1

Lutsko, N. J., Seeley, J. T., & Keith, D. W. (2020). Estimating impacts and tradeoffs in solar geoengineering scenarios with a moist energy balance model. *Geophysical Research Letters*, *47*, e2020GL087290. doi: 10.1029/2020GL087290

Manabe, S., & Stouffer, R. J. (1980). Sensitivity of a global climate model to an increase of CO2 concentration in the atmosphere. *Journal of Geophysical Research*, *85*(C10), 5529–5554. doi: 10.1029/JC085iC10p05529

Manabe, S., & Wetherald, R. T. (1975). The effects of doubling the CO2 concentration on the climate of a general circulation model. *Journal of the Atmospheric Sciences*, *32*(1), 3–15.

Merlis, T. M. (2014). Interacting components of the top-of-atmosphere energy balance affect changes in regional surface temperature. *Geophysical Research Letters*, *41*, 7291–7297. doi: 10.1002/2014GL061700

Merlis, T. M., & Henry, M. (2018). Simple estimates of polar amplification in moist diffusive energy balance models. *Journal of Climate*, *31*(15), 5811–5824. doi: 10.1175/JCLI-D-17-0578.1

North, G. R. (1975). Theory of energy-balance climate models. *Journal of the Atmospheric Sciences*, *32*(11), 2033–2043. doi: 10.1175/1520-0469(1975)032⟨2033:TOEBCM⟩2.0.CO;2

North, G. R., Cahalan, R. F., & Coakley, J. A. (1981). Energy balance climate models. *Reviews of Geophysics*, *19*(1), 91. doi: 10.1029/RG019i001p00091

O'Gorman, P. A., & Schneider, T. (2008). The hydrological cycle over a wide range of climates simulated with an idealized GCM. *Journal of Climate*, *21*(15), 3815–3832. doi: 10.1175/2007JCLI2065.1

Payne, A. E., Jansen, M. F., & Cronin, T. W. (2015). Conceptual model analysis of the influence of temperature feedbacks on polar amplification. *Geophysical Research Letters*, *42*(21), 9561–9570. doi: 10.1002/2015GL065889

Pithan, F., & Mauritsen, T. (2014). Arctic amplification dominated by temperature feedbacks in contemporary climate models. *Nature Geoscience*, *7*(3), 181–184. doi: 10.1038/ngeo2071

Roe, G. H., Feldl, N., Armour, K. C., Hwang, Y.-T., & Frierson, D. M. W. (2015). The remote impacts of climate feedbacks on regional climate predictability. *Nature Geoscience*, *8*(2), 135–139. doi: 10.1038/ngeo2346

Rose, B. E. J., Armour, K. C., Battisti, D. S., Feldl, N., & Koll, D. D. B. (2014). The dependence of transient climate sensitivity and radiative feedbacks on the spatial pattern of ocean heat uptake. *Geophysical Research Letters*, *41*. doi: 10.1002/2013GL058955

Russotto, R. D., & Biasutti, M. (2020). Polar amplification as an inherent response of a circulating atmosphere: Results from the TRACMIP aquaplanets. *Geophysical Research Letters*, *47*(6), e2019GL086771. doi: 10.1029/2019GL086771

Sellers, W. D. (1969). A global climatic model based on the energy balance of the Earth-atmosphere system. *Journal of Applied Meteorology*, *8*(3), 392–400. doi: 10.1175/1520-0450(1969)008⟨0392:agcmbo⟩2.0.co;2

Wagner, T. J. W., & Eisenman, I. (2015). How climate model complexity influences sea ice stability. *Journal of Climate*, *28*(10), 3998–4014. doi: 10.1175/jcli-d-14-00654.1

Winton, M. (2006). Amplified Arctic climate change: What does surface albedo feedback have to do with it? *Geophysical Research Letters*, *33*(3). doi: 10.1029/2005GL025244

Yoshimori, M., Abe-Ouchi, A., & Laîné, A. (2017). The role of atmospheric heat transport and regional feedbacks in the Arctic warming at equilibrium. *Climate Dynamics*, *49*(9-10), 3457–3472. doi: 10.1007/s00382-017-3523-2

Zhang, X., Schneider, T., Shen, Z., Pressel, K., & Eisenman, I. (submitted). Seasonal cycle of idealized polar clouds: Large eddy simulations driven by a GCM. *Journal of Advances in Modeling Earth Systems*.